Microscopic description of orbital-selective spin ordering in $BaMn_2As_2$

L. Craco[1,2] and S. S. Carara[1]

[1]*Instituto de Física, Universidade Federal de Mato Grosso, 78060-900, Cuiabá, MT, Brazil*

[2]*IFW Dresden, Institute for Solid State Research, P.O. Box 270116, D-01171 Dresden, Germany*

(Received 7 February 2018; revised manuscript received 10 April 2018; published 10 May 2018)

Using generalized gradient approximation+dynamical mean-field theory, we provide a microscopic description of orbital-selective spin ordering in the tetragonal manganese pnictide $BaMn_2As_2$. We demonstrate the coexistence of local moments and small band-gap electronic states in the parent compound. We also explore the role played by electron/hole doping, showing that the Mott insulating state is rather robust to small removal of electron charge carriers similar to cuprate oxide superconductors. Good qualitative accord between theory and angle-resolved photoemission as well as electrical transport provides support to our view of orbital-selective spin ordering in $BaMn_2As_2$. Our proposal is expected to be an important step to understanding the emergent correlated electronic structure of materials with persisting ordered localized moments coexisting with Coulomb reconstructed nonmagnetic electronic states.

DOI: 10.1103/PhysRevB.97.205114

I. INTRODUCTION

Superconductivity with high transition temperatures (high-T_c), observed layered cuprates [1], and various classes (including 11, 122 chacogenides and 122, 1111 pnictides) [2] of iron-based superconductors highlights the importance of electron correlation effects in unconventional (non-BCS) superconductors. Both superconducting families share common planar building blocks of stacked square layers of transition-metal ions. However, the parent compounds of Cu-based superconductors are known to be Mott insulators with strong Coulomb correlations [3], while the parent iron-based superconductors are either metallic, semiconducting, or pseudo-gapped electronic systems in their normal state [2,4]. La_2CuO_4, for example, is a local magnetic moment antiferromagnetic (AFM) insulator while $BaFe_2As_2$ is metallic with an AFM ordering characterized as a spin-density wave arising from mobile carriers. Moreover, in contrast to the cuprates, iron-based superconductors are multiorbital (MO) systems with the whole $3d^6$ manifold being relevant to intrinsic electronic and magnetic properties [5]. As a result of changing the band filling upon electron/hole doping, the two families share low coherence energy scales but they differ on the degree of electron correlation effects.

In view of the fact that superconductivity in both families arises from quantum many-particle fluctuations in the normal state, the importance of understanding the physical properties of parent compounds to rationalize the different mechanisms responsible for the superconducting state has been recognized. Based on this, in recent years there has been a growing interest to characterize materials which share similar properties which might provide a bridge to understanding the unconventional Cooper pairing phenomena in non-Fermi liquids in its broad sense. With this in mind, in this paper we investigate the electronic and magnetic properties of pure and doped $BaMn_2As_2$, which is isostructural to the iron-based superconducting compound $BaFe_2As_2$. However, different from this iron arsenide, the Mn^{2+} shell hosts five electrons instead of six Fe electrons in the five active $3d$ orbitals crossing the Fermi energy. It is noteworthy here that electron-electron interactions are expected to reach maximum at half-filling and to decrease away from this configuration [6]. In the case of tetragonal, transition-metal arsenides, this behavior is consistent with the observation by angle-resolved photoemission spectroscopy (ARPES) of reduced electronic correlations in $BaCo_2As_2$ as compared to $BaFe_2As_2$ [7], evidence which was inferred from a smaller renormalization of the correlated electronic structure in the former case. However, how MO interactions, expected to be larger for the half-filled ($3d^5$) shell of $BaMn_2As_2$, affect the electronic reconstruction in the magnetically ordered state has not been completely understood theoretically. Here we report a generalized gradient approximation+dynamical mean-field theory (GGA+DMFT) study of $BaMn_2As_2$ in view of describing how the interplay between MO electron-electron interactions and the half-filled Mn-$3d$ manyfold promotes narrow-gap Mott physics and the formation of strongly localized moments within the magnetically ordered state of pure and doped $BaMn_2As_2$.

Apart from the $3d$-band filling, $BaMn_2As_2$ is closely related to the parent compounds of the iron-arsenide superconductors and it also shows local moment AFM order, similar to parent cuprate superconductors. For both the 122 iron-pnictides and high-T_c copper oxides, superconductivity usually arises upon suppression of the long-range AFM order via chemical substitution or pressure effects [2,4,8,9]. Thus, since $BaMn_2As_2$ shares characteristics of both high-T_c superconducting families, it is expected to represent an important bridge between them and might shed new light on the nature of superconductivity in these and related compounds [10]. Electrical resistivity and specific-heat measurements on $BaMn_2As_2$ single crystals revealed that this compound is a small-band-gap ($E_{gap} \approx 0.05\,eV$) insulator [11]. Below the Néel temperature ($T_N = 625$ K), $BaMn_2As_2$ shows a collinear (G-type) AFM structure, where nearest-neighbor Mn moments in the

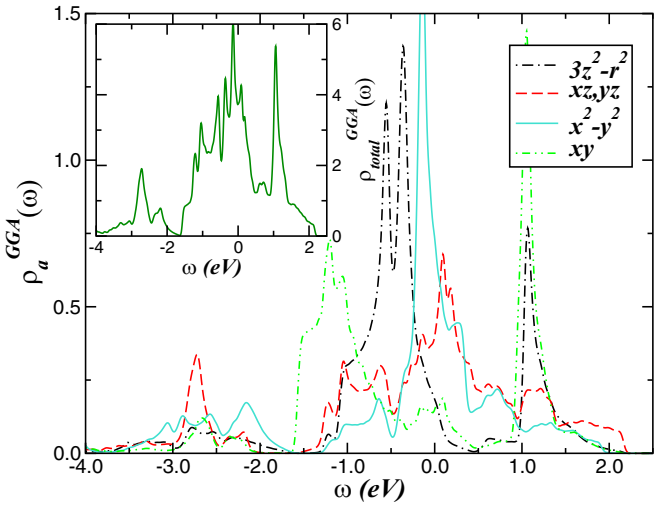

FIG. 1. GGA orbital-resolved (main panel) and total (inset) density of states (DOS) of paramagnetic $BaMn_2As_2$. Notice the multi-orbital anisotropies in the bare electronic structure, a characteristic shared with all tetragonal iron-based superconductors.

tetragonal basal plane are antiparallel with an ordered moment of $3.88(4)\mu_B$/Mn aligned along the c axis [10]. While no superconducting state has been found conclusively in spite of a sharp fall in resistivity at low temperatures in pressurized and K-doped $BaMn_2As_2$ [12,13], the manganese pnictides still show fascinating physical properties such as coexistence of AFM-ordered localized Mn spins and conduction carries in K-doped samples [14], half-metallic itinerant ferromagnetism with local-moment antiferromagnetism [12] as well the presence of robust AFM spin waves across the metal-insulator transition in hole-doped samples [15]. Finally, efforts to induce metallicity by pressure or doping the Mn parent compound have been successful [12,13,16–18], providing a route to explore novel physical properties in this class of strongly correlated d-band materials.

II. THEORY AND RESULTS

Extant theoretical understanding of tetragonal $BaMn_2As_2$ is based on *ab initio* local density approximation (LDA) and GGA calculations, [17,19,20], LDA+Gutzwiller method with electron density self-consistency [21], and GGA+DMFT [22,23] for both the paramagnetic and magnetically ordered state. Specifically, and similar to iron-based superconducting materials, *ab initio* density-functional calculations for paramagnetic $BaMn_2As_2$ demonstrate that the As-4p states lie well below the Fermi energy (E_F) and are weakly hybridized with Mn 3d states [23]. Hence, the most relevant electronic states near E_F derive from Mn^{2+} shell with almost direct Mn-Mn hopping. To confirm this scenario, we undertook GGA calculations [24] for the nonmagnetic parent compound using realistic lattice structural parameters [10]. The corresponding orbital-resolved GGA density of states (DOS) is shown in the main panel of Fig. 1. In good agreement with previous one-electron band structure calculations [23], our results (see inset of Fig. 1) confirm that the active electronic states involve the Mn 3d carriers. The MO anisotropies in the GGA band structure are also clearly manifested in Fig. 1. As common to all Fe-based superconductors, the $3z^2-r^2$,xy orbitals exhibit the bonding/antibonding splitting characteristic of the tetragonal unit cell. In contrast to these orbitals, which are almost band gapped, the x^2-y^2 band shows dominant electronic contribution near E_F, suggesting enhanced electronic localization within the paramagnetic normal state (not shown). Needless to say, a proper microscopic description of delocalization-localization transition with increasing the on-site Coulomb interaction U and the possibility of finding an orbital-selective insulating regime within the AFM-ordered state of $BaMn_2As_2$ is important for understanding the role played by dynamical correlations in the low-energy electronic excitations of iron-based superconductors and analogs [29]. In this paper, we provide microscopic new insights to the problem of MO electron-electron interactions in AFM $BaMn_2As_2$, revealing the emergence of orbital-selective magnetism [30,31] and its possible implications to Mott-like physics with coexisting strongly localized moments and narrow-gapped electronic states.

The MO Hamiltonian relevant for $BaMn_2As_2$ [22,23] is $H = H_0 + H_{\rm int}$ with $H_0 = \sum_{\mathbf{k}a\sigma} \epsilon_a(\mathbf{k}) c^\dagger_{\mathbf{k}a\sigma} c_{\mathbf{k}a\sigma}$, and $H_{\rm int} = U\sum_{ia} n_{ia\uparrow}n_{ia\downarrow} + \sum_{ia\neq b} U' n_{ia}n_{ib} - J_H \sum_{ia\neq b} \mathbf{S}_{ia}\cdot\mathbf{S}_{ib}$. Here, $a = x^2-y^2, 3z^2-r^2, xz, yz, xy$ label the diagonalized 3d orbitals of $BaMn_2As_2$ and $\epsilon_a(\mathbf{k})$ is the one-electron band dispersion, which encodes details of the one-electron (GGA) band structure. $U' \equiv U - 2J_H$, with U,U' being the intra- and interorbital Coulomb repulsion and J_H is the Hund's rule coupling. We evaluate the many-particle Green's functions of the Hamiltonian above for the AFM-ordered state within GGA+DMFT [32], using MO iterated perturbation theory as the impurity solver [33]. The DMFT solution involves replacing the lattice model by a self-consistently embedded MO-Anderson impurity model, and the self-consistency condition requiring the local impurity Green's function to be equal to the local Green's function for the lattice. The full set of equations for the MO case can be found in Ref. [33], so we do not repeat the equations here.

Since the dependence of electron-electron interactions in the excitation spectrum of magnetically ordered MO systems is quite subtle and not yet fully understood, in Fig. 2 we display the excitation spectrum that emerges from dynamical MO electron-electron interactions in AFM BaM_2As_2. To proceed, we follow the strategy used earlier [20,23], where calculations of the electronic band structure were performed within the G-type AFM magnetic order observed experimentally [10]. Moreover, to derive this ordered state, we use the GGA DOS shown in Fig. 1 as input to the GGA+DMFT calculations [34]. It is noteworthy, however, that due to the G-type ordering, the magnetic unit cell is doubled in the z direction in $BaMn_2As_2$. This implies that in the AFM phase, the period of the unit cell of the lattice is doubled due to the reduced translational symmetry. Consequently, the volume of the magnetic Brillouin zone is reduced to one-half of the volume in the paramagnetic state [35]. These changes in the symmetries across the magnetic phase transition can be taken into account by introduction of an AB-sublattice structure and reformulating the theory for the paramagnetic state [5] on an enlarged unit cell containing two sublattices, A and B, for all orbitals with components

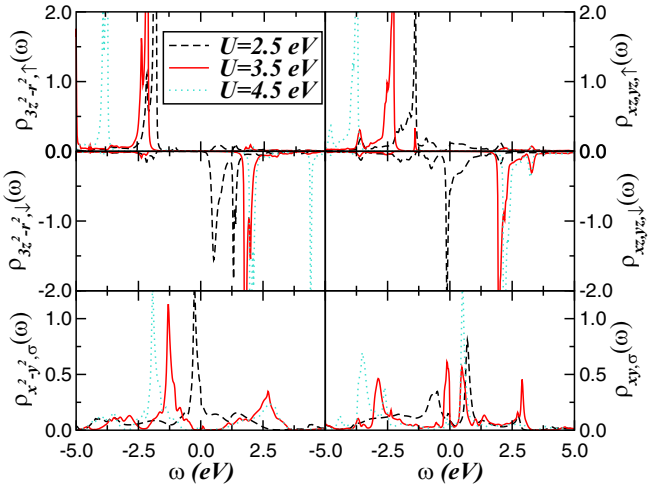

FIG. 2. GGA+DMFT orbital- and spin-resolved DOS of $BaMn_2As_2$. Notice the electronic reconstruction within the planar x^2-y^2,xy orbitals with increasing the on-site Coulomb interaction U (and fixed $J_H = 0.7$ eV). Particularly interesting is the formation of strongly localized moments within the $3z^2-r^2,xz,yz$ orbitals and their dynamical downshift toward high-binding energies with increasing U. The negative value of the DOS for the $3z^2-r^2,xz,yz$ orbitals refers to the opposite spin.

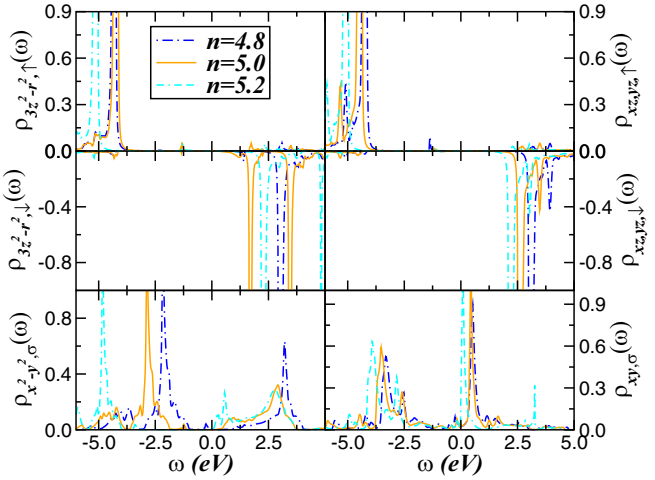

FIG. 3. Effect of electron and hole doping on the GGA+DMFT ($U = 5.0$ eV and $J_H = 0.7$ eV) orbital- and spin-resolved DOS of $BaMn_2As_2$. Notice the large transfer of spectral weight and the appearance of lower and upper Hubbard bands of the planar x^2-y^2,xy bands at different energies. A particularly interesting feature to be seen is the coexistence of insulating (x^2-y^2) and metallic (xy) states in electron-doped $BaMn_2As_2$. As in Fig. 2, the negative value of DOS refers to the opposite spin.

pointing along the z direction. Therefore, in the search for a G-type ordered phase in pure and doped $BaMn_2As_2$, one needs to extend the bipartite Green's function formalism for the one- and three-band Hubbard models [35,36] to the corresponding MO case, assuming the $3z^2-r^2,xz,yz$ orbitals to be magnetically ordered in $BaMn_2As_2$. In this regime, the retarded, one-particle Green's function at site A or $B(A/B)$, orbital $\alpha = 3z^2-r^2,xz,yz$, and spin σ reads [34]

$$G^{A/B}_{\alpha\sigma} = \int_{-\infty}^{\infty} d\varepsilon \rho^{\rm GGA}_{\alpha}(\varepsilon) \frac{\xi^{B/A}_{\alpha\sigma}(\omega)}{\xi^{A}_{\alpha\sigma}(\omega)\xi^{B}_{\alpha\sigma}(\omega) - \varepsilon^2} \, .$$

Here $\xi^{A/B}_{\alpha\sigma}(\omega) = \omega + \mu - \Sigma^{A/B}_{\alpha\sigma}(\omega)$, with $\rho^{\rm GGA}_{\alpha}(\varepsilon)$ and $\Sigma_{\alpha}(\omega)$ being, respectively, the GGA DOS (see Fig. 1) and the self-energy of orbital α, and μ the chemical potential of the system. For the sake of simplicity, in the AFM state it is sufficient to perform calculations for the A-sublattice due to the additional symmetry $G^{A}_{\alpha\sigma} = G^{B}_{\alpha\bar{\sigma}}$ of the bipartite lattice [35], and the planar x^2-y^2,xy orbitals are assumed by construction to be non-spin-polarized.

We now discuss our results for the G-type Néel ordered state of $BaMn_2As_2$, focusing our attention on the one-particle MO spectrum of the A-sublattice [$\rho_{\alpha,\sigma}(\omega) \equiv -\frac{1}{\pi} Im G^{A}_{\alpha\sigma}(\omega)$]. To begin with, let us first describe the electronic reconstruction with increasing the on-site Coulomb interaction U of the non-spin-polarized (x^2-y^2,xy) orbitals in Fig. 2. Our results in these orbital sectors for three different U values and fixed $J_H = 0.7$ eV (our choice for J_H is consistent with values used in earlier studies for $BaMn_2As_2$ [22,23] and iron-based superconductors [5]), reveal the formation of a Mott-Hubbard gap at low energies with concomitant appearance of lower and upper Hubbard bands at high energies. As seen, electron-electron interactions strongly modify the GGA spectral functions: MO dynamical correlations arising from U,U' and J_H lead to spectral weight redistribution over large energy scales. Noticeable differences in the spectral weight transfer are seen between the x^2-y^2 and xy channels. While the x^2-y^2 orbital is Mott localized for $U = 3.5$ eV, the xy band displays an incoherent, pseudogaplike metallic state with residual DOS at E_F up to $U = 4.5$ eV. This orbital-selective behavior is expected to be seen in MO systems close to Mott localization. However, more interesting is the electronic reconstruction within the spin-polarized electronic states where the spectral functions show sharp localized moments in the majority (spin-$\uparrow$) channels and the emergent orbital differentiation of the minority (spin-$\downarrow$) channels with increasing U.

This spin-polarized electronic scenario is robust upon increasing the on-site Coulomb repulsion to 5.0 eV, as shown in Fig. 3. Interestingly, however, is the appearance of an insulating electronic state with distinct band gaps near E_F in the planar bands. While the $3x^2-y^2$ orbital display pronounced Mott localization, the xy orbital shows a narrow V-shaped electronic band gap at E_F for $BaMn_2As_2$ parent compound, $n = 5$. Based on our results in Figs. 2 and 3, we thus predict that strong orbital reconstruction occurs at the correlation-induced Mott metal-insulator transition of $BaMn_2As_2$. Our GGA+DMFT results in Fig. 3 are consistent with extant ARPES, [20], suggesting large rearrangement of electronic states at low and high energies. Particularly interesting is the peak in the electronic DOS that develops around 3.0 eV, which, according to our theory, arises from the electronic structure of the nonmagnetically ordered x^2-y^2,xy orbitals. Additionally relevant in Ref. [20] is the observation of two hole bands with distinct one-band gaps in accord with our GGA+DMFT result for $n = 5$. Consistent with this ARPES data, the narrow band gap found in the xy

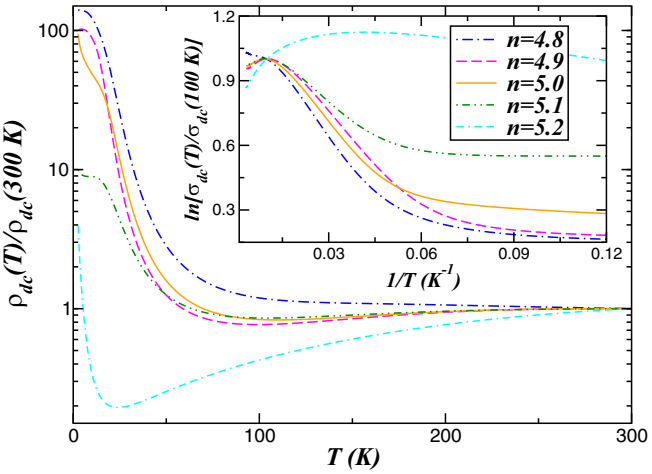

FIG. 4. Effect of electron/hole doping on the electrical resistivity ($\rho_{\rm dc}$) of the $U = 5.0$ eV antiferromagnetic ordered state of $BaMn_2As_2$. Notice the semiconductinglike resistivity in the hole-doped regime and the appearance of a Kondo-like resistivity upturn for $n = 5.2$. Inset shows our results for $ln(\sigma_{\rm dc})$ versus inverse temperature $(1/T)$, consistent with extant experimental data [10].

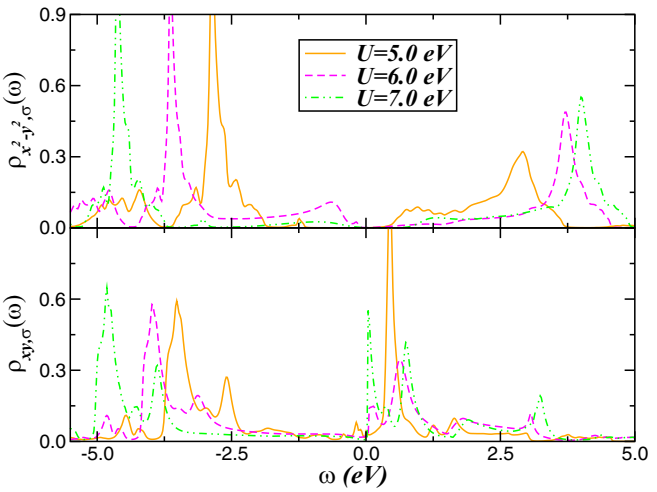

FIG. 5. Effect of on-site Coulomb interaction U on the non-spin-polarized electronic states of $BaMn_2As_2$ parent compound. Notice the large transfer of spectral weight yielding orbital-differentiated localization effects in these two planar bands. A particularly interesting feature to be seen in future XAS experiments on strained $BaMn_2As_2$ is the low-energy electronic reconsctrucition of the xy conduction band states, where the narrow peak at $\omega \approx 0.45$ eV is split into two with increasing U.

channel also clarifies why $BaMn_2As_2$ parent compound has a metalliclike in-plane resistivity above a sample dependent temperature between 50 K to 100 K [10,19], providing further support to our GGA+DMFT description of orbital-selective spin ordering in $BaMn_2As_2$.

To gain insights on the interplay between electron-electron interactions and electron/hole doping on the multiple structure of the AFM-ordered state of $BaMn_2As_2$, in Fig. 3 we also display our GGA+DMFT ($U = 5.0$ eV and $J_H = 0.7$ eV) for two distinct values of the d-shell occupancy, n. Large spectral weight transfer is visible upon addition/removal of charge carries in the magnetically ordered state of $BaMn_2As_2$. Particularly interesting is the Mott insulating state within the $x^2 - y^2$ sector, which is robust against small electron/hole doping. Also relevant is the shoulder in the conduction band states of the xy orbital, which crosses E_F at $n = 5.2$. This in turn induces band metallicity in this in-plane orbital channel. Thus, our results suggest the coexistence of distinct electronic degrees of freedom at low energies in doped $BaMn_2As_2$. This behavior is expected in MO Mott systems close to electronic delocalization, where strong orbital and spin fluctuations prevent the metallic Fermi liquid fixed point. Our work calls for future ARPES and polarized optical studies on electron-doped $BaMn_2As_2$. These studies will constitute a proof to anisotropic electronic delocalization and nonglobal electron-frozen antiferromagnetism as well as the importance of treating dynamical correlations adequately to reveal a variety of unexplored responses in correlated narrow-band materials close to metal-insulator instabilities.

Let us now discuss the implications of our results to electrical transport experiments [10,19]. Here we recall that the electrical resistivity ($\rho_{\rm dc}$) is directly computable from the MO GGA+DMFT propagators [37]. As a result, in Fig. 4 we show the T-dependence of $\rho_{\rm dc}(T)$ for different band fillings. A semiconducting behavior with small activation energy [10] is obtained for $n = 5.0$, as expected from our result for $U = 5.0$ eV in Fig. 3. Similar to cuprate oxide superconductors [38], the insulating behavior persists at small hole-doping concentrations in $BaMn_2As_2$. Interesting as well is the saturated low-T regime with decreasing n, which is caused by residual electronic states close to E_F in the xy orbital, as shown in Fig. 3. On the other hand, the localized Mott state gives away with increasing temperature and a crossover to metallic behavior characterized by a positive coefficient in $\rho_{\rm dc}(T)$ is found for $n \geqslant 4.9$, a behavior, which is also seen in experiments [10,19]. However, due to strong electronic reconstruction at low energies in electron-doped $BaMn_2As_2$, where the conduction band shoulder in the xy orbital spans the Fermi energy, this crossover scale, which is marked by the minimum of $\rho_{\rm dc}(T)$ with increasing T is found to be near to 20 K for $n = 5.2$. Albeit, no experimental evidence exists to date; our results suggest that electron-doped $BaMn_2As_2$ hosts a Kondo-like insulating behavior [39] with a resistivity upturn [40] below a characteristic energy scale, and future experiments on electron-doped samples are called for to put our prediction on solid ground. Finally, in the inset of Fig. 4 we make contact with an experiment on $BaMn_2As_2$ [10], showing qualitative good agreement with calculations for $ln(\sigma_{\rm dc})$ versus $1/T$, with $\sigma_{\rm dc}(T)$ being the electrical conductivity. Particular features to be seen in our results are the smooth $1/T$-dependence for $n = 4.9$ and the changes in slope for $n = 5.0$ which are, respectively, seen in $BaMn_2As_2$ grown samples using MnAs and Sn flux. Also relevant is the behavior at low $1/T$ values where the maximum in $ln(\sigma_{\rm dc})$ is found to be in good accord with experimental data. This, together with the positive temperature coefficien,t supports the view that $BaMn_2As_2$ is a bad metal [10] above a characteristic (sample dependent) temperature with rather small mean free paths for the conduction carriers due to intrinsically narrow-band-gapped xy electronic states.

In view of the above and on previous GGA+DMFT studies on strained graphene systems, [34,41] we now attempt to predict features of the physical responses owing to the orbital-dependent behavior of the non-spin-polarized electronic state of strained $BaMn_2As_2$. We recall here that the bare one-particle bandwidth W is expected to reduce when the Mn ions are pulled far apart under strong negative pressure conditions. This in turn will increase the U/W ratio or the effective on-site Coulomb interaction, inducing enhanced electron correlation effects in the system. With this in mind, in Fig. 5, we show the changes in the x^2-y^2,xy spectral functions of $BaMn_2As_2$ parent compound with increasing U. An orbital differentiation phenomenon [42] is clearly visible in Fig. 5, whereby Mott localization is stronger on the x^2-y^2 orbital as compared to the xy orbital yielding large spectral weight transfer from low to high energies. We propose that future polarized photoemission and x-ray absorption spectroscopy (XAS) experiments, which probe one-electron subtraction and addition spectra, could directly see these features in strained $BaMn_2As_2$ samples. In particular, the low-energy electronic reconstruction within the xy orbital, where the localized peak found at $\omega \approx 0.45$ eV for $U = 5.0$ eV splits into two with concomitant appearance of a broad incoherent peak just above E_F at large U values, $U \geqslant 6.0$ eV. Taken together with our results in Fig. 3, the most salient feature to be seen in Fig. 5 is the changes in the xy conduction band states above E_F. We predict that room temperature polarized XAS and/or resonant x-ray diffraction measurements would show up in an electronic reconstruction in strained $BaMn_2As_2$ as in Fig. 5. This could be tested in future experimental works.

III. CONCLUSION

In conclusion, we have performed GGA+DMFT calculations for the MO Hubbard model to provide a microscopic description of the excitation spectrum which emerges in the G-type AFM-ordered state of $BaMn_2As_2$. We show how MO electron-electron interactions induce an electronic state characterized by coexisting ordered magnetic moments and Mott-localized electronic states. Since $BaMn_2As_2$ is an insulator at low temperatures, our results demonstrate that antiferromagnetism arises from ordering of local Mn moments instead of from itinerant carriers as commonly attributed to metallic iron-based superconductors. Additionally, we have explored the role played by electron/hole doping the parent compound, showing that the Mott insulating state is robust against small hole doping similar to cuprate superconductors [43]. The good qualitative accord between our theoretical results with extant angle-resolved photoemission and electrical transport provides support to our proposal of orbital-selective spin ordering in $BaMn_2As_2$, suggesting that a similar mechanism could be found in the AFM-ordered state of iron-based superconductors. Our microscopic description of coupled MO Hubbard interactions is expected to be generally applicable to understanding orbital-selective magnetism [30,31] in strongly correlated electron systems and the underlying electronic state which might emerge in magnetically ordered superconductors [44].

ACKNOWLEDGMENT

L.C.'s work is supported by CNPq (Grant No. 304035/2017-3).

[1] M. Imada, A. Fujimori, and Y. Tokura, Rev. Mod. Phys. **70**, 1039 (1998).

[2] D. C. Johnston, Adv. Phys. **59**, 803 (2010); G. R. Stewart, Rev. Mod. Phys. **83**, 1589 (2011); K. Deguchi, Y. Takano, and Y. Mizuguchi, Sci. Technol. Adv. Mater. **13**, 054303 (2012); M. K. Wu, P. M. Wu, Y. C. Wen, M. J. Wang, P. H. Lin, W. C. Lee, T. K. Chen, and C. C. Chang, J. Phys. D: Appl. Phys. **48**, 323001 (2015); Q. Si, R. Yu, and E. Abrahams, Nat. Rev. Mater. **1**, 16017 (2016).

[3] P. A. Lee, N. Nagaosa, and X.-G. Wen, Rev. Mod. Phys. **78**, 17 (2006).

[4] J. Paglione and R. L. Greene, Nat. Phys. **6**, 645 (2010).

[5] K. Haule, J. H. Shim, and G. Kotliar, Phys. Rev. Lett. **100**, 226402 (2008); L. Craco, M. S. Laad, S. Leoni, and H. Rosner, Phys. Rev. B **78**, 134511 (2008).

[6] L. de' Medici, G. Giovannetti, and M. Capone, Phys. Rev. Lett. **112**, 177001 (2014).

[7] N. Xu, P. Richard, A. van Roekeghem, P. Zhang, H. Miao, W.-L. Zhang, T. Qian, M. Ferrero, A. S. Sefat, S. Biermann, and H. Ding, Phys. Rev. X **3**, 011006 (2013).

[8] P. Dai, Rev. Mod. Phys. **87**, 855 (2015).

[9] S. A. J. Kimber, A. Kreyssig, Y.-Z. Zhang, H. O. Jeschke, R. Valenti, F. Yokaichiya, E. Colombier, J. Yan, T. C. Hansen, T. Chatterji, R. J. McQueeney, P. C. Canfield, A. I. Goldman, and D. N. Argyriou, Nat. Mater. **8**, 471 (2009).

[10] Y. Singh, M. A. Green, Q. Huang, A. Kreyssig, R. J. McQueeney, D. C. Johnston, and A. I. Goldman, Phys. Rev. B **80**, 100403(R) (2009).

[11] Y. Singh, A. Ellern, and D. C. Johnston, Phys. Rev. B **79**, 094519 (2009).

[12] A. Pandey, B. G. Ueland, S. Yeninas, A. Kreyssig, A. Sapkota, Yang Zhao, J. S. Helton, J. W. Lynn, R. J. McQueeney, Y. Furukawa, A. I. Goldman, and D. C. Johnston, Phys. Rev. Lett. **111**, 047001 (2013).

[13] A. T. Satya, A. Mani, A. Arulraj, N. V. Chandra Shekar, K. Vinod, C. S. Sundar, and A. Bharathi, Phys. Rev. B **84**, 180515(R) (2011).

[14] S. Yeninas, A. Pandey, V. Ogloblichev, K. Mikhalev, D. C. Johnston, and Y. Furukawa, Phys. Rev. B **88**, 241111(R) (2013).

[15] M. Ramazanoglu, A. Sapkota, A. Pandey, J. Lamsal, D. L. Abernathy, J. L. Niedziela, M. B. Stone, A. Kreyssig, A. I. Goldman, D. C. Johnston, and R. J. McQueeney, Phys. Rev. B **95**, 224401 (2017).

[16] K. Zhao, Z. Deng, X. C. Wang, W. Han, J. L. Zhu, X. Li, Q. Q. Liu, R. C. Yu, T. Goko, B. Frandsen, L. Liu, F. Ning, Y. J. Uemura, H. Dabkowska, G. M. Luke, H. Luetkens, E. Morenzoni, S. R. Dunsiger, A. Senyshyn, P. Böni, and C. Q. Jin, Nat. Commun. **4**, 1442 (2013).

[17] J.-K. Bao, H. Jiang, Y.-L. Sun, W.-H. Jiao, C.-Y. Shen, H.-J. Guo, Y. Chen, C.-M. Feng, H.-Q. Yuan, Z.-A. Xu, G.-H. Cao,

R. Sasaki, T. Tanaka, K. Matsubayashi, and Y. Uwatoko, Phys. Rev. B **85**, 144523 (2012).

[18] A. Pandey, R. S. Dhaka, J. Lamsal, Y. Lee, V. K. Anand, A. Kreyssig, T. W. Heitmann, R. J. McQueeney, A. I. Goldman, B. N. Harmon, A. Kaminski, and D. C. Johnston, Phys. Rev. Lett. **108**, 087005 (2012).

[19] J. An, A. S. Sefat, D. J. Singh, and M.-H. Du, Phys. Rev. B **79**, 075120 (2009).

[20] W.-L. Zhang, P. Richard, A. van Roekeghem, S.-M. Nie, N. Xu, P. Zhang, H. Miao, S.-F. Wu, J.-X. Yin, B. B. Fu, L.-Y. Kong, T. Qian, Z.-J. Wang, Z. Fang, A. S. Sefat, S. Biermann, and H. Ding, Phys. Rev. B **94**, 155155 (2016).

[21] Y. X. Yao, J. Schmalian, C. Z. Wang, K. M. Ho, and G. Kotliar, Phys. Rev. B **84**, 245112 (2011).

[22] D. E. McNally, S. Zellman, Z. P. Yin, K. W. Post, H. He, K. Hao, G. Kotliar, D. Basov, C. C. Homes, and M. C. Aronson, Phys. Rev. B **92**, 115142 (2015).

[23] M. Zingl, E. Assmann, P. Seth, I. Krivenko, and M. Aichhorn, Phys. Rev. B **94**, 045130 (2016).

[24] To gain realistic insights into the multiorbital electronic structure of $BaMn_2As_2$ on a microscopic level, we performed density-functional band-structure calculations as implemented in the SIESTA simulation package [25]. We used generalized gradient approximation (GGA) with the Perdew-Burke-Ernzerhof [26] exchange-correlation functional with norm-conserving Troullier-Martins pseudopotentials [27]. The charge density was represented on a real-space grid with an energy cutoff of 200 Ry. The reciprocal space was sampled with a fine $15 \times 15 \times 15$ Monkhorst-Pack k-point grid [28].

[25] J. M. Soler, E. Artacho, J. D. Gale, A. García, J. Junquera, P. Ordejón, and D. Sánchez-Portal, J. Phys.: Condens. Matter **14**, 2745 (2002).

[26] J. P. Perdew, K. Burke, and M. Ernzerhof, Phys. Rev. Lett. **77**, 3865 (1996).

[27] N. Troullier and J. L. Martins, Phys. Rev. B **43**, 8861 (1991).

[28] H. J. Monkhorst and J. D. Pack, Phys. Rev. B **13**, 5188 (1976).

[29] V. K. Anand and D. C. Johnston, Phys. Rev. B **94**, 014431 (2016); J. Fink, E. D. L. Rienks, S. Thirupathaiah, J. Nayak, A. van Roekeghem, S. Biermann, T. Wolf, P. Adelmann, H. S. Jeevan, P. Gegenwart, S. Wurmehl, C. Felser, and B. Büchner, *ibid.* **95**, 144513 (2017); M. Edelmann, G. Sangiovanni, M. Capone, and L. de' Medici, *ibid.* **95**, 205118 (2017); S. Lee, G. A. de la Pena, S. X.-L. Sun, Y. Fang, M. Mitrano, H. Jang, J.-S. Lee, C. Eckberg, D. Campbell, J. Collini, J. Paglione, F. M. F. de Groot, and P. Abbamonte, arXiv:1801.04874.

[30] M. Yi, Y. Zhang, Z.-X. Shen, and D. Lu, Quantum Mater. **2**, 57 (2017).

[31] J. M. Caron, J. R. Neilson, D. C. Miller, K. Arpino, A. Llobet, and T. M. McQueen, Phys. Rev. B **85**, 180405(R) (2012).

[32] G. Kotliar, S. Y. Savrasov, K. Haule, V. S. Oudovenko, O. Parcollet, and C. A. Marianetti, Rev. Mod. Phys. **78**, 865 (2006).

[33] L. Craco, Phys. Rev. B **77**, 125122 (2008).

[34] L. Craco, Phys. Rev. B **96**, 165412 (2017).

[35] Th. Maier, M. B. Zölfl, Th. Pruschke, and J. Keller, Physica B: Condens. Matter **259–261**, 747 (1999).

[36] L. Craco and M. A. Gusmão, Phys. Rev. B **54**, 1629 (1996).

[37] L. Craco and S. Leoni, Sci. Rep. **7**, 46439 (2017).

[38] L. Craco, Phys. Rev. B **79**, 085123 (2009), and references therein.

[39] J. Kondo, Prog. Theor. Phys. **32**, 37 (1964).

[40] Y. Katayama and S. Tanaka, Phys. Rev. **153**, 873 (1967); Y. Xu, J. Zhang, G. Cao, C. Jing, and S. Cao, Phys. Rev. B **73**, 224410 (2006).

[41] L. Craco, D. Selli, G. Seifert, and S. Leoni, Phys. Rev. B **91**, 205120 (2015); L. Craco, S. S. Carara, and S. Leoni, *ibid.* **94**, 165168 (2016).

[42] H. Miao, Z. P. Yin, S. F. Wu, J. M. Li, J. Ma, B.-Q. Lv, X. P. Wang, T. Qian, P. Richard, L.-Y. Xing, X.-C. Wang, C. Q. Jin, K. Haule, G. Kotliar, and H. Ding, Phys. Rev. B **94**, 201109(R) (2016).

[43] T.-P. Choy and P. Phillips, Phys. Rev. Lett. **95**, 196405 (2005).

[44] F. Waß er, C. H. Lee, K. Kihou, P. Steffens, K. Schmalzl, N. Qureshi, and M. Braden, Sci. Rep. **7**, 10307 (2017); W.-H. Jiao, Q. Tao, Z. Ren, Y. Liu, and G.-H. Cao, Quantum Materials **2**, 50 (2017).